ChemComm

Nonmetallic Metal toward Pressure-Induced Bad-Metal State in Two-Dimensional Cu3LiRu2O6

Journal:	*ChemComm*
Manuscript ID	CC-COM-08-2019-006691.R1
Article Type:	Communication

COMMUNICATION

Nonmetallic Metal toward Pressure-Induced Bad-Metal State in Two-Dimensional $Cu_3LiRu_2O_6$

Received 00th January 20xx,
Accepted 00th January 20xx

DOI: 10.1039/x0xx00000x

Bin Huang,[a] Ziyi Liu,[b] Yifeng Han,[a] Shuang Zhao,[a] Meixia Wu,[a] Corey E. Frank,[c] Martha Greenblatt,[c] Mark Croft,[d] Nicholas F. Quackenbush,[e] Sizhan Liu,[f] Trevor A. Tyson,[f] Lei Zhang,[g] Junliang Sun,[g] Peifei Shan,[b,h] Jianhong Dai,[b] Xiaohui Yu,[b,h,i] Jinguang Cheng,[*b,h,i] Man-Rong Li[a,*]

The novel two-dimensional honeycomb layered $Cu_3LiRu_2O_6$ exhibits Pauli-like paramagnetic and Mott variable range hopping semiconduction behaviors, which contradict the large specific-heat Sommerfeld coefficient for metals, and indicate a possible spin-excitation induced nonmetallic metal. This nonmetallic feature can be significantly suppressed toward a bad-metal state by pressure, as reflected from the temperature-dependent resistivity response up to 35 GPa.

Introduction

Materials based on the delafossite modified structures have exhibited interesting physical properties and important applications, such as photocatalytic activity, thermoelectric behavior, transparent conductor, and measurement-based quantum computation.[1-3] The crystal structure of delafossite ABO_2 consists of two-dimensional (2D) edge-sharing BO_6 octahedral planes separated by intercalated linear-dumbbell A-cations.[4] It can be modified to be A_2BO_3- or $A_3A'B_2O_6$-type when intralayer disordering is introduced. [1, 5-16] Recently, exotic physical phenomena have been manifested in modified delafossites with 4d/5d transition metals at the B-site, particularly because of strong spin-orbit coupling (SOC) coexisting with other competing interactions and geometric frustration inherent for the honeycomb layers. Mott and metal-insulator transitions have been reported in modestly frustrated A_2RuO_3 (A = Li, Na),[8-10] while highly anisotropic Kitaev interactions rooted in the difference of electron configuration and SOC between Ru^{4+} ($4d^4$, S = 1) and Ir^{4+} ($5d^5$, S = 1/2) were proposed in the iridates Na_2IrO_3 and Li_2IrO_3.[7] Exotic low energy excitations have been observed in the random Kitaev magnet Cu_2IrO_3.[17, 18] Quantum spin liquid state has been, for the first time, discovered in the quaternary 3R-delafossite $A_3A'B_2O_6$-type $H_3LiIr_2O_6$,[6, 19] which suggests that the electronic and magnetic properties of delafossite can be largely tuned by cationic substitution.

In the modified delafossite $A_3A'B_2O_6$, higher degree of complication arises when two types of cations are ordered in the triangular layer, as in quaternary 3R-delafossite $A_3MB_2O_6$. In comparison with ABO_2 delafossite, lattice disorder in $A_3MB_2O_6$ disturbs the periodic potential and thus places interference on electron waves,[20, 21] and makes the materials highly 2D in nature.[12, 14] This scenario can lead to dramatic changes of physical properties as observed in ruthenate-based modified delafossites, implying that the electronic and magnetic properties of modified delafossites can be refined by substitution of the inter- and/or intra-layer cations, and are worthy of further exploration.[16] In this work, we prepared a novel modified delafossite, $Cu_3LiRu_2O_6$, via topotactic soft chemistry synthesis from Li_2RuO_3 (**Fig. S1**), and studied its crystal structure, magnetic response, specific heat, and pressure-dependent resistivity in detail.

The crystal structure determination of modified delafossite is challenging due to the complicated layer-stacking fault.[15] Refinements of the synchrotron powder x-ray diffraction (SPXD) data of $Cu_3LiRu_2O_6$ were carried out in $C2/m$ (No. 12, as in Ag_3LiRuO_6 and $Ag_3LiMn_2O_6$)[11, 14] and $C2/c$(No. 15, as in $Cu_3LiIr_2O_6$ and Cu_2IrO_3),[16, 17] respectively. Acceptable goodness of fitting was observed in both cases, but with the $C2/m$ model giving better agreement overall (**Fig. 1**, R_{wp}/R_p = 5.65/6.92%) than the $C2/c$ (**Fig. S2**, R_{wp}/R_p = 6.82/9.43%) model. Therefore, the $C2/m$

[a.] Key Laboratory of Bioinorganic and Synthetic Chemistry of Ministry of Education, School of Chemistry, Sun Yat-Sen University, Guangzhou 510275, P. R. China.
[b.] Beijing National Laboratory for Condensed Matter Physics and Institute of Physics, Chinese Academy of Sciences, Beijing 100190, P. R. China
[c.] Department of Chemistry and Chemical Biology, Rutgers, The State University of New Jersey, 610 Taylor Road, Piscataway, New Jersey 08854, United States.
[d.] Department of Physics and Astronomy, Rutgers, the State University of New Jersey,136 Frelinghuysen Road, Piscataway, New Jersey 08854, United States.
[e.] Materials Measurement Science Division, Material Measurement Laboratory, National Institute of Standards and Technology, Gaithersburg, Maryland 20899, United States.
[f.] Department of Physics, New Jersey Institute of Technology, Newark, New Jersey 07102, United States.
[g.] College of Chemistry and Molecular Engineering, Peking University, Beijing 100871, P. R. China
[h.] School of Physical Sciences, University of Chinese Academy of Sciences, Beijing 100190, P. R. China
[i.] Songshan Lake Materials Laboratory, Dongguan 523808, P. R. China
Electronic Supplementary Information (ESI) available: [details of any supplementary information available should be included here]. See DOI: 10.1039/x0xx00000x

cell (a = 5.2085(2) Å, b = 9.0236(2) Å, c = 6.0267(2) Å, β = 106.59(1)°, V = 271.42(2) Å^3, Z = 2) was used to describe the crystal structure of $Cu_3LiRu_2O_6$. As can be seen in **Fig. 1**, an asymmetric broad feature (Warren-line shape)[22] of peaks appears around 8-11 degrees, which is characteristic of 2D structural order with stacking faults in the *c* direction as further corroborated by the streaking diffraction peaks in selected-area electron diffraction (SAED) patterns (**Fig. S3**, [$\bar{1}$10] reciprocal lattice plane along the stacking direction).[23] The detailed crystallographic parameters, bond valence sums (BVS) calculations, and octahedral distortion parameters (Δ) are listed in **Tables S1-S2**. Both BVS (**Table S2**) and x-ray absorption near-edge spectroscopy (XANES, **Figure S9-S10**) studies imply Ru^{4+} and Cu^{+} dominated valence in $Cu_3LiRu_2O_6$.

Fig. 2 shows the magnetization curves of $Cu_3LiRu_2O_6$ at different magnetic fields ($H_{0\mu}$ = 0.1, 1, 5 T). Unlike the strongly AFM (T_N ~ 15 K) spin coupling in $Cu_3LiIr_2O_6$,[16] no evidence for long-range magnetic order or spin freezing was detected down to 2 K in $Cu_3LiRu_2O_6$; instead the susceptibility keeps temperature-independent between 80 - 300 K, revealing a Pauli-like paramagnetic behavior of metals caused by the reaction of the conduction electrons to the applied field. The full-range susceptibility can be fitted by the equation of $\chi = \chi_0 + C/(T - \theta)$ with the temperature independent contribution χ_0, the Curie-Weiss temperature θ_{CW} and the Curie constant C. A least-square fit gives χ_0 = 0.0039 emu/mol Oe, θ_{CW} = -2.54 K, and C = 0.028 K emu/mol Oe. From the value of C, the resulting magnetic moment μ_{eff} is 0.47 μ_B in $Cu_3LiRu_2O_6$ at 0.1 T magnetic field, which is much smaller than the expected free-ion value of 2.83 μ_B for Ru^{4+} (effective S = 1). It is the electron correlations among the electrons in the narrow π* conduction band of t_{2g} parentage that give rise to such a weak Curie-Weiss term in $Cu_3LiRu_2O_6$, resembling those of $LaNiO_3$[24], $BaNbO_3$[25] and $Sr_4V_3O_{9.60}$.[26] Note that the molar magnetic susceptibility as a function of magnetic field was investigated at 2 K, which veers off a straight line, indicating the presence of ferromagnetic impurities in $Cu_3LiRu_2O_6$ (inset of **Fig. 2a**). Thus, as the magnetic field is increased, the susceptibility of $Cu_3LiRu_2O_6$ is slightly decreased and the μ_{eff} (0.49 μ_B when μ_0H = 1 T and 0.54 μ_B when μ_0H = 5 T) subtly increased.

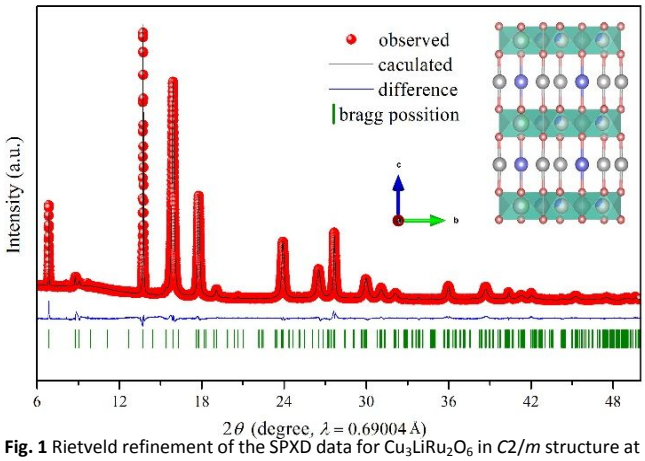

Fig. 1 Rietveld refinement of the SPXD data for $Cu_3LiRu_2O_6$ in *C*2/*m* structure at RT. Inset shows the crystal structure viewed along [100] direction, Cu1, gray spheres; Cu2, blue spheres; $(Li/Ru)O_6$ octahedra, green.

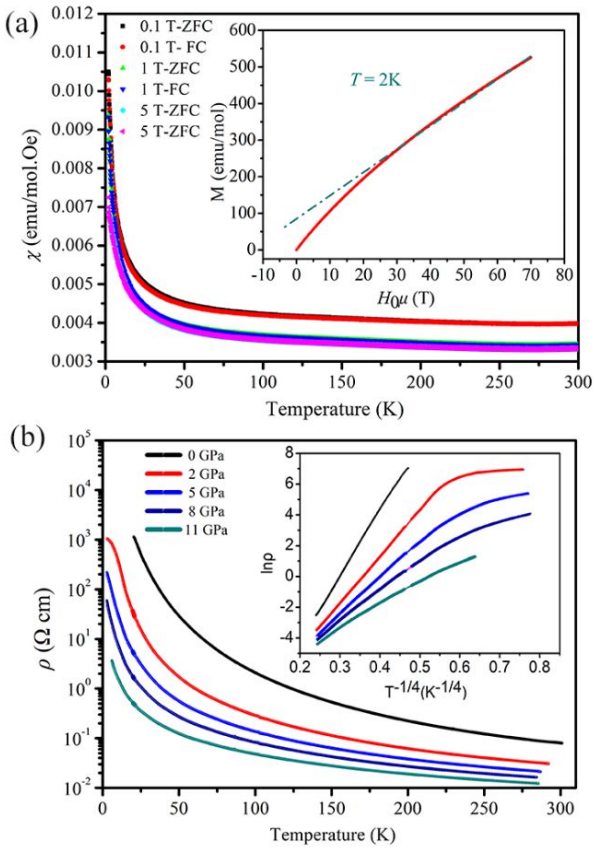

Fig.2 (a)Magnetization curves of $Cu_3LiRu_2O_6$ at different magnetic fields ($H_{0\mu}$ = 0.1, 1, 5 T). Inset shows the molar magnetic susceptibility as a function of magnetic field intensity was invested at 2 K, where the observed and fitted lines are shown in red and green, respectively. (b)Temperature dependence of resistivity $\rho(T)$ under various pressures up to 11 GPa for a $Cu_3LiRu_2O_6$ polycrystalline sample, inset shows lnρ versus $T^{-1/4}$ plots for the $\rho(T)$ data.

The temperature dependence of resistivity $\rho(T)$ for $Cu_3LiRu_2O_6$, shown in **Fig. 2b**, increases substantially on cooling with no obvious transition. At approximately room temperature (RT) ρ (0.09(1) Ω.cm) is comparable to that of $Ag_3LiRu_2O_6$ (0.01 Ω.cm),[12] close to what has been observed in bad metals, but ~ 300 times lower than that of Li_2RuO_3 (~ 30 Ω.cm).[10] At 10 K, $Cu_3LiRu_2O_6$ becomes more insulating, and the resistivity rises to ~ 3000 Ω.cm, which is about four orders of magnitude higher than that at RT. The $\rho(T)$ curve can be well described by Mott's three-dimensional variable range hopping (VRH) model, i.e. $\rho = \rho_0 \exp(T/T_0)^{-1/4}$, in which T_0 is the activation energy. As illustrated in the inset of **Fig. 2b**, the plot of lnρ versus $T^{-1/4}$ produces linear behavior and the slope corresponds to the Mott activation energy, T_0.

Fig. 3a displays the temperature dependence of specific heat, $C(T)$, measured at 0 and 8 T, respectively. No obvious anomaly can be discerned in the studied temperature range 2-200 K, signaling the absence of phase transition, in agreement with the magnetic susceptibility results. We found that the $C(T)$ data in the measured temperature range can be well described by considering one Debye (Θ_D = 287 K) and two Einstein modes (Θ_{E1} = 113 K, Θ_{E2} = 633 K), as illustrated by the dotted line. As can be seen, the application of 8 T external magnetic field has a marginal effect and only modifies $C(T)$ slightly at low

temperatures. The $C(T)$ data below 10 K were replotted in **Fig. 3b** in the form of C/T versus T^2, and a linear fitting $C/T = \gamma + \beta T^2$ was applied to extract the linear specific-heat coefficient γ and the Debye temperature $\Theta_D = (12p^4nR/5\beta)^{1/3}$, where $n = 12$ is the number of atoms in the formula unit, and $R = 8.3145$ J/mol-K is the ideal gas constant. Interestingly, we observe a large linear specific-heat Sommerfeld coefficient $\gamma = 41.7(5)$ and $47.9(4)$ mJ/mol-K^2 for 0 and 8 T, respectively, suggesting metallic behavior, which contradicts the VRH semiconducting resistivity behavior in **Fig. 2b**. Although the presence of magnetic Ru^{4+} ions might give rise a magnetic contribution to specific heat at low temperature, the observation of nearly temperature-independent magnetic susceptibility and perfect overlap of ZFC/FC for $\chi(T)$ rules out the presence of localized moments and spin-liquid or spin-glass states. In this regard, $Cu_3LiRu_2O_6$ may belong to the novel family of nonmetallic metals as reported in $Lu_2Rh_2O_7$[27] and FeCrAs, considering their common features.[28-31]

Nonmetallic metals present three common features: triangular magnetic lattice and temperature independent Pauli paramagnetic response, large Sommerfeld coefficient γ, and a gap in the density of states (negative slope of $\rho(T)$ curve).[27-30] The triangular motifs enable geometric magnetic frustration, which corresponds to the corner-sharing tetrahedral sublattice in pyrochlore $Lu_2Rh_2O_7$, the distorted Kagome Cr-network in FeCrAs, and the honeycomb Ru-layer in $Cu_3LiRu_2O_6$. A hidden spin liquid state[29] or Hund's metal[32] behavior is proposed by researchers to explain the nonmetallic metal response in FeCrAs, while inelastic neutron scattering suggests that the high energy itinerant-like spin excitation accounts for the nonmetallic resistivity in FeCrAs[27, 30] as also proposed for $Lu_2Rh_2O_7$.[27] Considering the similarity of 4*d*-electron character between Ru and Rh, it is most likely spin excitation that is responsible for the nonmetallic metal behavior in $Cu_3LiRu_2O_6$, which requires further corroboration from spin dynamics measurements on large single crystals. Alternatively, the presence of large amount of lattice disorders and grain boundaries can produce potentials, which localize the charge carriers with Anderson localization effect.[33] Here, the Anderson localization scenario seems unlikely due to the absence of large magnetoresistance, or clean signals of non-fermi-liquid behavior.[34, 35]

For materials with competing ground states, pressure is a powerful tool to refine the balance between SOC, Coulomb repulsion, and crystal field interactions for novel phenomena as observed in layered ruthenates and iridates.[36, 37] **Fig. 2b** shows $\rho(T)$ measured up to 11 GPa for $Cu_3LiRu_2O_6$. The resistivity

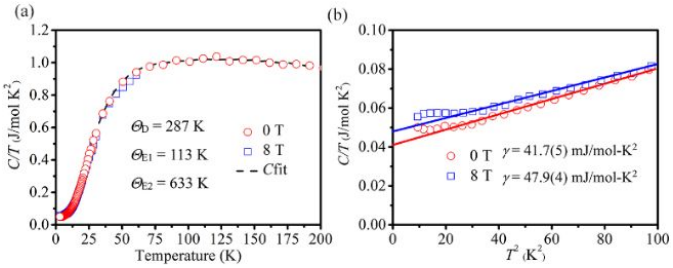

Fig.3 (a) Temperature dependence of specific heat $C(T)$ for $Cu_3LiRu_2O_6$ under 0 T and 8 T, (b) the low-temperature $C(T)$ data in the form of C/T vs T^2.

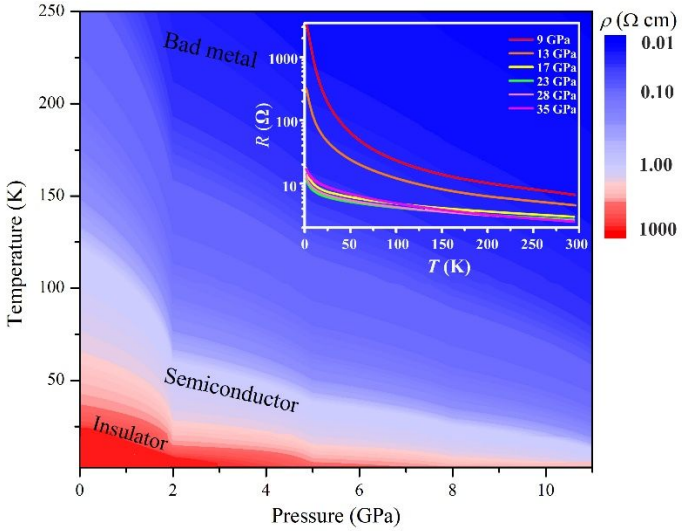

Fig.4 Temperature- and pressure-dependent resistivity phase diagram of $Cu_3LiRu_2O_6$. Inset shows the *R-T* plots measured between 9 and 35 GPa. A contour fill of the resistivity data is superimposed on the phase diagram.

decreases gradually with increasing pressure in the whole temperature range. At RT, the resistivity is ~ 10 times smaller (0.01(1) Ω.cm) under 11 GPa than that (0.09(1) Ω.cm) at 0 GPa. The resistivity is significantly reduced at lower temperatures and higher pressures, being three orders of magnitude smaller (1.62(1) Ω.cm) under 11 GPa than that at 0 GPa (~ 3000 Ω.cm) at 10 K. All observed resistivity behaviors can be well explained by Mott's VRH mechanism as shown in the inset of **Fig. 2b**, where the slope that reflects the Mott activation energy T_0, decreases gradually with increasing pressure. The reduction of T_0 with pressure may be attributed to the intrinsic suppression of the band gap under pressure, in addition to an improvement of the grain connection for the studied polycrystalline sample. The schematic temperature- and pressure-dependent resistivity phase diagram is shown in **Fig. 4**. Apparently, the nonmetallic state in $Cu_3LiRu_2O_6$ can be strongly suppressed under pressure. However, a true metallic state cannot be achieved up to 35 GPa, the highest pressure in the present study, as shown in the inset of **Fig. 4**, where resistance (R) keeps decreasing at higher pressure (9-28 GPa) but starts to increase when pressed above 28 GPa as discovered in other 4*d*/5*d*-transition metal oxides.[38]The temperature-dependent *R-T* plots at higher-pressure region (inset of **Fig. 4**) cannot be well fitted and explained by any thermal activation model, indicating that the sample enters a conductive or bad-metal state. Further investigations are need to examine if much higher pressures are required to drive $Cu_3LiRu_2O_6$ into a true metallic state.[39]

In summary, we have prepared a new modified delafossite-type $Cu_3LiRu_2O_6$ via soft topotactic reaction, and extensively characterized the crystal structure and physical properties. Both magnetic susceptibility and specific heat measurements on $Cu_3LiRu_2O_6$ demonstrate strong electron correlations, giving temperature-independent Pauli-like paramagnetic behavior and large Sommerfeld coefficient γ. However, resistivity

measurements show that $Cu_3LiRu_2O_6$ is insulating at room temperature and follows Mott variable range hopping semiconducting behavior to low temperature. The contradiction suggests that $Cu_3LiRu_2O_6$ is a nonmetallic metal, probably attributed to spin excitation. Temperature-dependent resistivity measurements up to 35 GPa reveal that the nonmetallic state in $Cu_3LiRu_2O_6$ can be significantly suppressed by pressure, indicating a possible pressure-driven bad-metal state at higher pressure. Our results show that $Cu_3LiRu_2O_6$ is the second nonmetallic metal oxide beside $Lu_2Rh_2O_7$. In addition, these findings imply that the physical properties of delafossite can be largely tuned by isovalent substitution of both the *A*- and *B*- site ions, and the resultant properties can be very subtly affected by ionic radii, electron configuration of the constituent TM, and lattice distortion as reflected by the differences between $Cu_3LiRu_2O_6$ and $Li_3LiRu_2O_6$ (Li_2RuO_3), $Ag_3LiRu_2O_6$, and $Cu_3LiIr_2O_6$.

Conflicts of interest

There are no conflicts to declare.

Notes and references

1. K. Ramesha, A. S. Prakash, M. Sathiya, G. Madras and A. K. Shukla, *Mater. Sci. Eng. B*, 2011, **176**, 141-146.
2. I. Terasaki, S. Abe, Y. Yasui, R. Okazaki and H. Taniguchi, *J. Mater. Chem. C*, 2015, **3**, 10430-10435.
3. H. Kawazoe, M. Yasukawa, H. Hyodo, M. Kurita, H. Yanagi and H. Hosono, *Nature*, 1997, **389**, 939-942.
4. J. Chaloupka, G. Jackeli and G. Khaliullin, *Phys. Rev. Lett.*, 2013, **110**, 097204.
5. G. Khaliullin, *Phys. Rev. Lett.*, 2013, **111**, 197201.
6. K. Kitagawa, T. Takayama, Y. Matsumoto, A. Kato, R. Takano, Y. Kishimoto, S. Bette, R. Dinnebier, G. Jackeli and H. Takagi, *Nature*, 2018, **554**, 341.
7. A. Kitaev, *Ann. Phys.*, 2006, **321**, 2-111.
8. J. C. Wang, J. Terzic, T. F. Qi, F. Ye, S. J. Yuan, S. Aswartham, S. V. Streltsov, D. I. Khomskii, R. K. Kaul and G. Cao, *Phys. Rev. B*, 2014, **90**, 161110.
9. A. C. W. P. James and J. B. Goodenough, *J. Solid State Chem.*, 1988, **74**, 287-294.
10. Y. Miura, Y. Yasui, M. Sato, N. Igawa and K. Kakurai, *J. Phys. Soc. Jpn.*, 2007, **76**, 033705.
11. R. Kumar, T. Dey, P. M. Ette, K. Ramesha, A. Chakraborty, I. Dasgupta, R. Eremina, S. Tóth, A. Shahee, S. Kundu, M. Prinz-Zwick, A. A. Gippius, H. A. K. von Nidda, N. Büttgen, P. Gegenwart and A. V. Mahajan, *Phys. Rev. B*, 2019, **99**, 144429.
12. S. A. J. Kimber, C. D. Ling, D. J. P. Morris, A. Chemseddine, P. F. Henry and D. N. Argyriou, *J. Mater. Chem.*, 2010, **20**, 8021-8025.
13. S. Bette, T. Takayama, V. Duppel, A. Poulain, H. Takagi and R. E. Dinnebier, *Dalton Trans.*, 2019, **48**, 9250-9259.
14. R. Kumar, T. Dey, P. M. Ette, K. Ramesha, A. Chakraborty, I. Dasgupta, J. C. Orain, C. Baines, S. Tóth, A. Shahee, S. Kundu, M. Prinz-Zwick, A. A. Gippius, N. Büttgen, P. Gegenwart and A. V. Mahajan, *Phys. Rev. B*, 2019, **99**, 054417.
15. V. Todorova, A. Leineweber, L. Kienle, V. Duppel and M. Jansen, *J. Solid State Chem.*, 2011, **184**, 1112-1119.
16. J. H. Roudebush, K. A. Ross and R. J. Cava, *Dalton Trans.*, 2016, **45**, 8783-8789.
17. M. Abramchuk, C. Ozsoy-Keskinbora, J. W. Krizan, K. R. Metz, D. C. Bell and F. Tafti, *J. Am. Chem. Soc.*, 2017, **139**, 15371-15376.
18. Y. S. Choi, C. H. Lee, S. Lee, S. Yoon, W. J. Lee, J. Park, A. Ali, Y. Singh, J.-C. Orain, G. Kim, J.-S. Rhyee, W.-T. Chen, F. Chou and K.-Y. Choi, *Phys. Rev. Lett.*, 2019, **122**, 167202.
19. S. Bette, T. Takayama, K. Kitagawa, R. Takano, H. Takagi and R. E. Dinnebier, *Dalton Trans.*, 2017, **46**, 15216-15227.
20. A. Lagendijk, B. v. Tiggelen and D. S. Wiersma, *Phys. Today*, 2009, **62**, 24-29.
21. P. W. Anderson, *Phys. Rev.*, 1958, **109**, 1492-1505.
22. D. Balzar, *J. Res. Nal. Inst. Stan.*, 1993, **98**, 321-353.
23. E. Climent-Pascual, P. Norby, N. H. Andersen, P. W. Stephens, H. W. Zandbergen, J. Larsen and R. J. Cava, *Inorg. chem.*, 2012, **51**, 557-565.
24. X. Q. Xu, J. L. Peng, Z. Y. Li, H. L. Ju and R. L. Greene, *Phys Rev B Condens Matter*, 1993, **48**, 1112-1118.
25. J. A. A. M.T. Casais', I. Rasines', M.A. Hidalgo, *Mater. Res. Bull.*, 1995, **30**, 201-208.
26. T. N. N.Suzukl, N.Yamamoto and T.Hioki, *Mat. Res. Bull .* 1991, **26**, 75-83.
27. A. M. Hallas, A. Z. Sharma, C. Mauws, Q. Chen, H. D. Zhou, C. Ding, Z. Gong, M. Tachibana, P. M. Sarte, J. P. Attfield, G. M. Luke and C. R. Wiebe, *npj Quant. Mater.*, 2019, **4**, 9.
28. W. Wu, A. McCollam, I. Swainson, P. M. C. Rourke, D. G. Rancourt and S. R. Julian, *Europhys. Lett.*, 2009, **85**, 17009.
29. J. G. Rau and H.-Y. Kee, *Phys. Rev. B*, 2011, **84**, 104448.
30. K. W. Plumb, C. Stock, J. A. Rodriguez-Rivera, J. P. Castellan, J. W. Taylor, B. Lau, W. Wu, S. R. Julian and Y.-J. Kim, *Phys. Rev. B*, 2018, **97**, 184431.
31. A. Akrap, Y. M. Dai, W. Wu, S. R. Julian and C. C. Homes, *Phys. Rev. B*, 2014, **89**, 125115.
32. A. H. Nevidomskyy and P. Coleman, *Phys. Rev. Lett.*, 2009, **103**, 147205.
33. E. Abrahams, P. W. Anderson, D. C. Licciardello and T. V. Ramakrishnan, *Phys. Rev. Lett.*, 1979, **42**, 673-676.
34. S. Süllow, I. Maksimov, A. Otop, F. J. Litterst, A. Perucchi, L. Degiorgi and J. A. Mydosh, *Phys. Rev. Lett.*, 2004, **93**, 266602.
35. A. Otop, S. Süllow, M. B. Maple, A. Weber, E. W. Scheidt, T. J. Gortenmulder and J. A. Mydosh, *Phys. Rev. B*, 2005, **72**, 024457.
36. D. A. Zocco, J. J. Hamlin, B. D. White, B. J. Kim, J. R. Jeffries, S. T. Weir, Y. K. Vohra, J. W. Allen and M. B. Maple, *J. Phys.: Condens. Matter*, 2014, **26**, 255603.
37. Z. Zhao, S. Wang, T. F. Qi, Q. Zeng, S. Hirai, P. P. Kong, L. Li, C. Park, S. J. Yuan, C. Q. Jin, G. Cao and W. L. Mao, *J. Phys.: Condens. Matter*, 2014, **26**, 215402.
38. D. Haskel, G. Fabbris, M. Zhernenkov, P. P. Kong, C. Q. Jin, G. Cao and M. van Veenendaal, *Phys. Rev. Lett.*, 2012, **109**, 027204.
39. Y. Zhou, B. Zhang, X. Chen, C. Gu, C. An, Y. Zhou, K. Cai, Y. Yuan, C. Chen, H. Wu, R. Zhang, C. Park, Y. Xiong, X. Zhang, K. Wang and Z. Yang, *Adv. Electron. Mater.*, 2018, **4**,1800155.

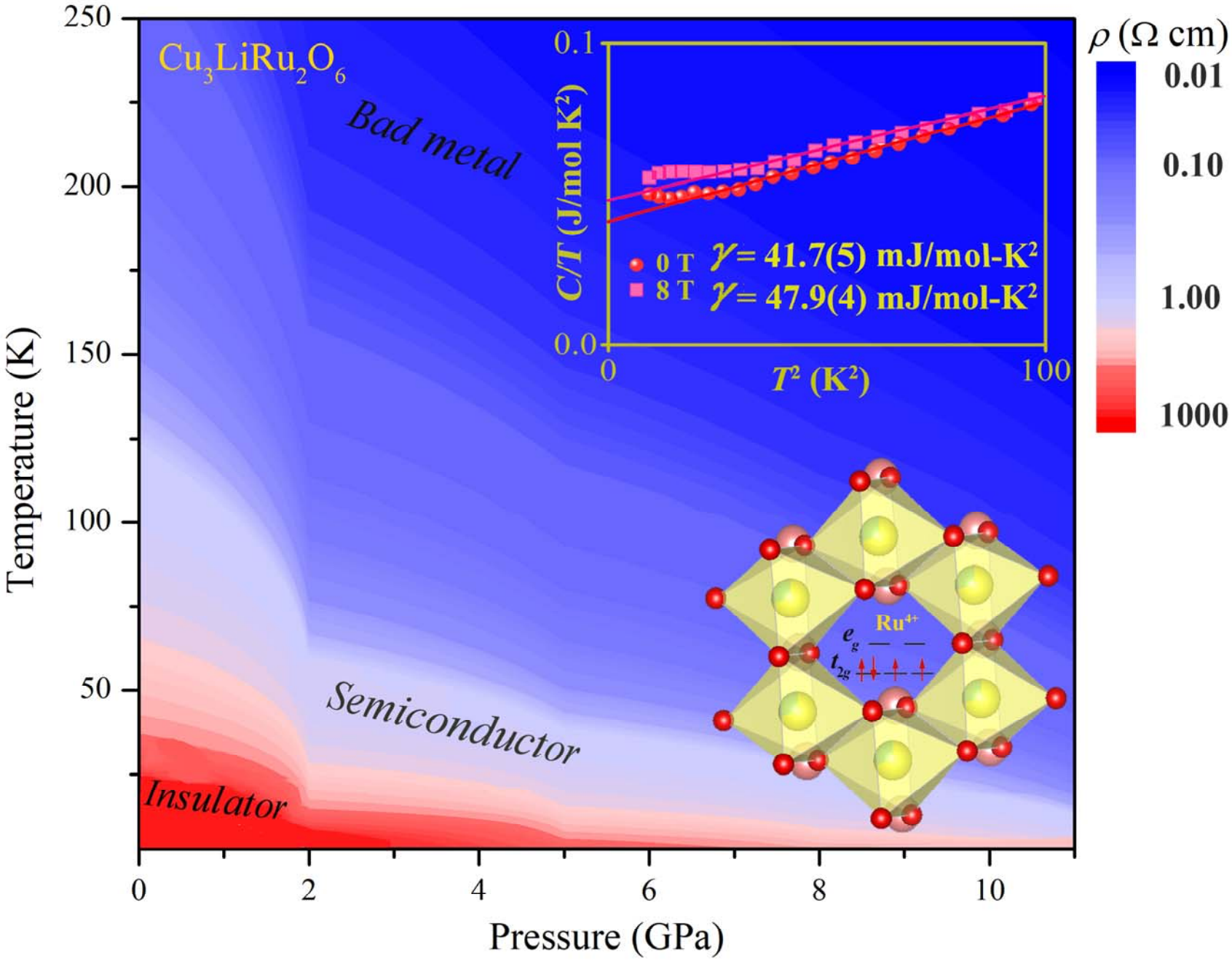
Cu3LiRu2O6
Bad metal
Semiconductor
Insulator
Temperature (K)
Pressure (GPa)
250
200
150
100
50
0
2
4
6
8
10
ρ (Ω cm)
0.01
0.10
1.00
1000
C/T (J/mol K²)
0.1
0.0
0
100
T² (K²)
0 T γ= 41.7(5) mJ/mol-K²
8 T γ= 47.9(4) mJ/mol-K²
Ru4+
eg
t2g